

Article

Weak Deflection Angle and Greybody Bound of Magnetized Regular Black Hole

Wajiha Javed ^{1,†} , Sibgha Riaz ^{1,†} and Ali Övgün ^{2,*,†} 

¹ Department of Mathematics, Division of Science and Technology, University of Education, Township Campus, Lahore 54590, Pakistan; wajiha.javed@ue.edu.pk (W.J.); sibghariaz993@gmail.com (S.R.)

² Physics Department, Eastern Mediterranean University, North Cyprus via Mersin 10, Famagusta 99628, Turkey

* Correspondence: ali.ovgun@emu.edu.tr

† These authors contributed equally to this work.

Abstract: In this paper, we examine the weak deflection angle and greybody bound for a magnetized regular black hole. For this purpose, we apply the Gauss–Bonnet theorem on the black hole and obtain the deflection angle in plasma and non-plasma mediums. Moreover, we investigate graphically the effect of impact parameter on the deflection angle for regular black hole in both mediums. We examine that the deflection angle goes to infinity when the impact parameter approaches zero. We also observe that the deflection angle shows negative behaviour at $q = 0.6$ and $q = 2.09$, but at $0.6 < q < 2.09$, the angle shows positive behaviour. Furthermore, we study the rigorous bound phenomenon of the greybody factor in the background for a magnetized regular black hole. Later, we analyse the graphical behaviour of greybody bound with respect to different values of ω and observe that, at small values of ω , the bound increases, but for large values, the bound decreases. After that, we examine that, when we put $G = 1$, $l = 0$ and $q = 0$, all results for the magnetized regular black hole solution reduce into results of the Schwarzschild black hole solution.



Citation: Javed, W.; Riaz, S.; Övgün, A. Weak Deflection Angle and Greybody Bound of Magnetized Regular Black Hole. *Universe* **2022**, *8*, 262. <https://doi.org/10.3390/universe8050262>

Academic Editors: Sunny Vagnozzi, Eleonora Di Valentino, Alessandro Melchiorri, Olga Mena, Luca Visinelli and Yi-Fu Cai

Received: 11 March 2022

Accepted: 22 April 2022

Published: 25 April 2022

Publisher's Note: MDPI stays neutral with regard to jurisdictional claims in published maps and institutional affiliations.



Copyright: © 2022 by the authors. Licensee MDPI, Basel, Switzerland. This article is an open access article distributed under the terms and conditions of the Creative Commons Attribution (CC BY) license (<https://creativecommons.org/licenses/by/4.0/>).

Keywords: general relativity; gravitational lensing; magnetized black holes; Gauss–Bonnet theorem; plasma medium; greybody factory

PACS: 95.30.Sf; 98.62.Sb; 97.60.Lf

1. Introduction

Black holes—a great prediction of Einstein's theory of general relativity (GR) and, at the same time, the understandable objects inside the universe—are of the utmost importance for classical and quantum gravity theories [1]. A region of space having such a strong gravitational field that matter or radiation, even light, cannot escape from it, is called a black hole (BH). Initially BHs were known as “Collapser”, the term derived from the collapse of a star; later, Wheeler put forward the term black hole [2]. A BH is an important tool for examining and testing the fundamental laws of the universe. In fact, the Event Horizon Telescope collaboration captured the first image of a BH [3].

In 1916, Einstein anticipated the existence of gravitational lensing (GL) and gravitational waves as part of the basics behind GR [1]. Recently, the gravitational waves were detected by the Laser Interferometer Gravitational Wave Observatory (LIGO) in 2015, which indicated that the theoretical predictions were well expressed with experimental observations [4]. After the detection of gravitational waves, a wide range of gravity theories faced many drawbacks, but the discovery of gravitational waves has gained interest in the field of GL [5]. As the light emitted by distant galaxies passes by massive objects in the universe, the gravitational pull from these objects can distort or bend the light. This is called gravitational lensing. Gravitational lensing is a helpful method to understand dark matter, galaxies, and the universe.

GL has been categorized in the literature as strong GL, weak GL, or micro GL [6–10]. The method which is used to observe the magnification and position of a BH is known as strong GL. The first strong GL for the Schwarzschild BH was performed by Virbhadra and Ellis [11]. Weak gravitational lensing (WGL) is an effective tool to measure the masses of different objects in the universe. Weak gravitational lensing investigates the cause of elevated enlargement of the universe and additionally distinguish among modified gravity and dark energy. Similarly, micro GL is worked on the bases of strong GL, in which the image separation is too small to be resolved. Gravitational lensing is processed in different space times in different ways [12–17]. Moreover, in past years, many studies have related GL with the Gauss–Bonnet theorem (GBT) after Gibbons and Werner’s conformation of the useful method for calculating the bending angle of BHs that shows asymptotic behaviour [18], which is given as:

$$\gamma = - \int \int_{D_\infty} \mathcal{K} dr,$$

where γ represents the deflection angle, \mathcal{K} represents the Gaussian optical curvature, dr represents the optical surface, and D_∞ symbolizes the infinite domain of the space.

Werner extended GBT method to a stationary BH [19]. Ishihara et al. [20] determined that it is possible to find a finite distance of deflection angle by using optical Fermat geometry. Crisnejo and Gallo [21] investigated the deflection angle of light in plasma medium. Since then, there has been a constantly increasing interest in the WGL through the Gibbons and Werner technique using GBT methodology for BHs and wormholes [22–29]. In addition, Hensh et al. [30] computed the GL of Kehagias–Sfetsos compact objects surrounded by plasma.

In 1974, Hawking predicted that BHs emit quantum radiation. Such radiation is known as Hawking radiation [31]. In the background of quantum field theory, the creation and annihilation of the particles is theoretically possible. When pair production takes place close to the horizon of a BH, one of the particles present in the pair production falls and the other particle leaves the horizon of a BH. An outside observer will detect this particle as Hawking radiation. However, according to GR, a BH bends spacetime around itself. This spacetime behaves like a gravitational potential for the particles to move. Few of the particles are reflected by the BH and remaining particles are transmitted through the BH. As a result, the Hawking radiation that the observer observes from outside the BH is distinct from the propagation through the gravitational potential. This distinction is known as the greybody factor. There are many studies investigating the computation of the greybody factor, such as the WKB approximation method [32–34]. Another attractive way to calculate the bound of the greybody factor is presented in [35–38].

Singularity has been a major problem since the beginning of history [39]. In GR, spacetime singularities increase several issues. Different techniques, such as nonlinear electrodynamics (NLED) and gravity modification, have been introduced to eliminate the spacetime singularities that occur at the centre of charged BHs. Born introduced the theory of NLED to solve point-like charge self-energy divergences and this theory was later modified with the help of Infield to establish the Born and Infield theory [40]. NLED models have received a lot of attention in recent years, with a lot of focus on their ability to discover regular BH solutions.

A magnetic black hole is a black hole with a magnetic charge. Magnetic black holes are permanent configurations compatible with the laws of physics. They have some interesting properties because they have large magnetic fields. Electro-weak symmetry can be restored around the black hole due to magnetized black hole. In astrophysics, magnetized black holes have received a lot of attention because they are supposed to be good models for realistic stellar-mass and supermassive black holes. Different methods have been proposed for obtaining electromagnetic energy from rotating magnetized black holes. The motion of charged particles in the vicinity of magnetic black holes, and its scattering and Hawking radiation, were all studied. It was shown that, in the presence of a magnetic

field, rotating black holes’ super-radiant instability and the intensity of Hawking evaporation are increased. It has recently been proposed that certain particle collisions in the presence of a weakly magnetized non-rotating black hole can produce particles with high centre-of-mass energy. Under some instances, magnetized non-rotating black holes could be used as particle accelerators. Exact solutions to the Einstein–Maxwell Equations [41] can help us understand black hole astronomy. The Harrison transformation was used to construct magnetized black hole solutions in 4-dimensional spacetime. They have recently been extended to a number of Einstein–Maxwell and Einstein–Maxwell-dilaton equations describing black objects in external magnetic fields in 5 dimensions. We believe it is critical to obtain further magnetic solutions because only the simplest solution can indicate a black hole on a gravitational instanton. A mathematical formulation for a black hole which does not contain a singularity is known as a regular black hole.

The main purpose of this paper is to analyse the magnetic regular black hole from global and analytical perspective in the presences of different mediums such as plasma and non-plasma using the Gauss–Bonnet theorem. Furthermore, we calculate the bound of greybody factor for magnetized regular black holes. We examine the graphically impact of bound and graphical behaviour of plasma and non-plasma mediums on the deflection angle.

This work is organized as follows: in Section 2, we study MRBH. In Section 3, by using GBT, we calculate the deflection angle in the background of non-plasma medium. In Section 4, we analyse the graphical behaviour of deflection angle in non-plasma medium. In Section 5, we compute the deflection angle for MRBH in plasma medium, and in Section 6 we study the graphical influence of deflection angle in plasma medium. In Section 7, we calculate the bound of greybody factor for MRBH. In Section 8, we observe the graphical impact of greybody bound. The last Section 9 is devoted to the conclusion.

2. Magnetized Regular Black Hole (MRBH)

A magnetic black hole is a black hole with a magnetic charge. Magnetic black holes are permanent configurations compatible with the laws of physics. They have some interesting properties because they have large magnetic fields. Electro-weak symmetry can be restored around the black hole due to magnetized black hole. In astrophysics, magnetized black holes have received a lot of attention because they are supposed to be good models for realistic stellar-mass and supermassive black holes. A mathematical formulation for a black hole which does not contain a singularity is known as regular black hole.

Kruglov used the following Lagrangian of nonlinear electrodynamics to obtain the magnetized regular black hole [42]:

$$\mathcal{L} = -\frac{\mathcal{F}}{1 + 2\beta\mathcal{F}} \tag{1}$$

with the following field tensor:

$$\mathcal{F} = (1/4)F_{\mu\nu}F^{\mu\nu} = (\mathbf{B}^2 - \mathbf{E}^2)/2, F_{\mu\nu} = \partial_\mu A_\nu - \partial_\nu A_\mu. \tag{2}$$

Note that the parameter β of the dimension of (length)⁴, and there is a Maxwell limit

$$\mathcal{L} \rightarrow -\mathcal{F}.$$

for weak fields $\beta\mathcal{F} \ll 1$. Then, using the above nonlinear electrodynamics fields, Kruglov derived the MRBH metric in spherically coordinates as follows [42]:

$$ds^2 = -H(r)dt^2 + \frac{dr^2}{H(r)} + r^2d\Omega_2^2, \tag{3}$$

where $H(r)$ can be defined as follows:

$$H(r) = 1 - \frac{2Gm}{r} + \frac{Gq^2}{r^2} + \frac{4G^2m^2l^2}{r^4} - \frac{4G^2ml^2q^2}{r^5} + \mathcal{O}(r^{-6}) \quad r \rightarrow \infty, \tag{4}$$

while

$$d\Omega_2^2 = d\theta^2 + \sin^2\theta d\phi^2. \tag{5}$$

Here, G is a Newton’s constant, l is the fundamental length, and m is the mass which is constant, and q is the magnetic charge. For equatorial plane $\theta = \frac{\pi}{2}$ and null geodesic $ds^2 = 0$, the optical metric is written as:

$$dt^2 = \frac{dr^2}{H(r)^2} + \frac{r^2d\phi^2}{H(r)}. \tag{6}$$

The non-zero Christoffel symbols of Equation (6) is calculated as:

$$\begin{aligned} \Gamma_{00}^0 &= -\frac{H'(r)}{H(r)}, \\ \Gamma_{10}^1 &= \frac{1}{r} - \frac{H'(r)}{2H(r)}, \\ \Gamma_{11}^0 &= \frac{-2H(r)}{r} + H'(r), \end{aligned} \tag{7}$$

in which 0 and 1 indicate r -coordinate and ϕ -coordinate, and the Ricci scalar of the optical metric computes as:

$$\mathcal{R} = H(r)H''(r) - \frac{(H'(r))^2}{2}. \tag{8}$$

The Gaussian curvature can be defined as given in the expression below:

$$\mathcal{K} = \frac{\text{Ricci Scalar}}{2}. \tag{9}$$

The required Gaussian optical curvature for the optical metric for MRBH is obtained as follows:

$$\begin{aligned} \mathcal{K} \approx & \frac{(3q^2 - 2mr)G}{r^4} + \frac{(-150mq^2 + 100m^2r + 2q^4r - 6mq^2r^2 + 3m^2r^3)G^2}{r^7} \\ - & \frac{2(47mq^4 + 9l^2mq^4 - 150m^2q^2r - 15l^2m^2q^2r + 78m^3r^2 + 6l^2m^3r^2)G^3}{r^9} \\ - & \frac{2(485m^2q^4 - 360l^2m^2q^4 - 780m^3q^2r + 600l^2m^3q^2r + 6mq^6r)G^4}{r^{12}} \\ - & \frac{2(-3l^2mq^6r + 312m^4r^2 - 240l^2m^4r^2 - 18m^2q^4r^2 + 9l^2m^2q^4r^2)G^4}{r^{12}} \\ - & \frac{2(18m^3q^2r^3 - 9l^2m^3q^2r^3 - 6m^4r^4 + 3l^2m^4r^4)G^4}{r^{12}}. \end{aligned} \tag{10}$$

3. Weak Deflection Angle for MRBH in Non-Plasma Medium

According to GBT, the topology of domain (\mathcal{S}_R) and the intrinsic structural of the spacetime are connected with boundary $\partial\mathcal{S}_R$. Then, with the help of GBT, the angle of deflection of the desired BH can be calculated as follows [18]:

$$\int \int_{\mathcal{S}_R} \mathcal{K}dS + \oint_{\partial\mathcal{S}_R} kdt + \sum_i \epsilon_i = 2\pi\mathcal{X}(\mathcal{S}_R), \tag{11}$$

the geodesic curvature, k , revealed as $k = \bar{g}(\nabla_{\dot{\beta}}\dot{\beta}, \dot{\beta})$, such that $\bar{g}(\dot{\beta}, \dot{\beta}) = 1$. If β is considered to be a smooth curve, then we obtain $\dot{\beta}$ as a unit speed vector, and ϵ_i represents the exterior angle at the i th vertex. As $R \rightarrow \infty$, we take $\pi/2$ as jump angle. This gives us $(\theta_S + \theta_O \rightarrow \pi)$.

$$\int \int_{S_R} \mathcal{K}dS + \oint_{\partial S_R} kdt + \epsilon_i = 2\pi\mathcal{X}(S_R), \tag{12}$$

Here, the total jump angle, presented by $\epsilon_i = \pi$. \mathcal{X} , is representing the Euler characteristic number which is 1. Geodesic curvature takes the form $k(C_R) = |\nabla_{\dot{P}_R}\dot{P}_R|$ that we will compute. The radial part mentioned in the geodesic curvature is calculated as:

$$(\nabla_{\dot{P}_R}\dot{P}_R)^r = \dot{P}_R^\phi \partial_\phi \dot{P}_R^r + \beta_{\phi\phi}^r (\dot{P}_R^\phi)^2. \tag{13}$$

For the high value of R , $P_R := r(\psi) = R = const$, where R shows the distance from the coordinate origin. Last expression $\beta_{\psi\psi}^r$ shows the Christoffel symbols in connection to the optical geometry. Due to the non-presence of the topological effect the first term present in the above expression vanishes while the second term takes the form $k(P_R) = |\nabla_{\dot{P}_R}\dot{P}_R|$ that shall be computed by using of unit speed term.

$$(\nabla_{\dot{P}_R}\dot{P}_R)^r \rightarrow \frac{1}{R}. \tag{14}$$

$k(P_R) \rightarrow R^{-1}$, due to absences of topological effect. By taking the advantage of the optical metric, it can be written as $dt = Rd\phi$. It can be stated that:

$$k(P_R)dt = \frac{1}{R}Rd\phi. \tag{15}$$

The following expression can be written when we collect all the above results:

$$\int \int_{S_R} \mathcal{K}ds + \oint_{\partial S_R} kdt \stackrel{R \rightarrow \infty}{=} \int \int_{O_\infty} \mathcal{K}dS + \int_0^{\phi+\gamma} d\phi. \tag{16}$$

The photon ray is expressed as $r(t) = b/\sin\phi$ at the 0th order in a weak field deflection limit. Therefore, the angle of deflection is defined as: ref. [18]

$$\gamma = - \int_0^\pi \int_{b/\sin\phi}^\infty \mathcal{K} \sqrt{\det\bar{g}} dr d\phi, \tag{17}$$

$\sqrt{\det\bar{g}}$ is calculated as:

$$\sqrt{\det\bar{g}} = r \left(1 - \frac{2Gm}{r} + \frac{Gq^2}{r^2} + \frac{4G^2m^2l^2}{r^4} - \frac{4G^2ml^2q^2}{r^5} \right) \tag{18}$$

By exploiting the above relation and putting the values of Gaussian curvature into Equation (17), the angle of deflection γ can be written as:

$$\begin{aligned} \gamma \approx & \frac{(4Gm)}{b} + \frac{(3G^2m^2\pi)}{4b^2} - \frac{(3Gq^2\pi)}{4b^2} - \frac{(8G^2mq^2)}{3b^3} - \frac{(75G^2m^2\pi)}{8b^4} \\ & - \frac{(45G^3m^2q^2\pi)}{32b^4} + \frac{(15G^2q^4\pi)}{64b^4} + \frac{(32G^2mq^2)}{b^5} + \frac{(12G^3mq^4)}{5b^5} \\ & + \frac{(125m^2G^3q^2\pi)}{8b^6} + \frac{(525G^4m^2q^4\pi)}{256b^6} - \frac{(4192G^3mq^4)}{245b^7} \\ & - \frac{(43155G^4m^2q^4\pi)}{2048b^8} + \frac{(6111G^4m^2q^4\pi)}{256b^{10}} + \frac{(567G^4l^2m^2q^4\pi)}{128b^{10}}. \end{aligned} \tag{19}$$

The deflection angle γ obtained in a non-plasma medium depends on the m of the BH, q , b , G , and l . We observe that in the attained deflection angle the first term is the well-known result for the Schwarzschild black hole, when we put $G = 1, l = 0, q = 0$.

4. Graphical Representation for Non-Plasma of MRBH

This section is for the graphical impact of the deflection angle γ on MRBH. The physical importance of the graphs is studied also, in order to analyse the effect of different parameters on the achieved angle by allocating different values to BH charge, impact parameters, and fundamental length.

4.1. Angle of Deflection γ versus Impact Parameter b

Figure 1 shows the conduct of γ with respect to b by taking the fix value of $m = 1, G = 1$, and varying q and l , respectively.

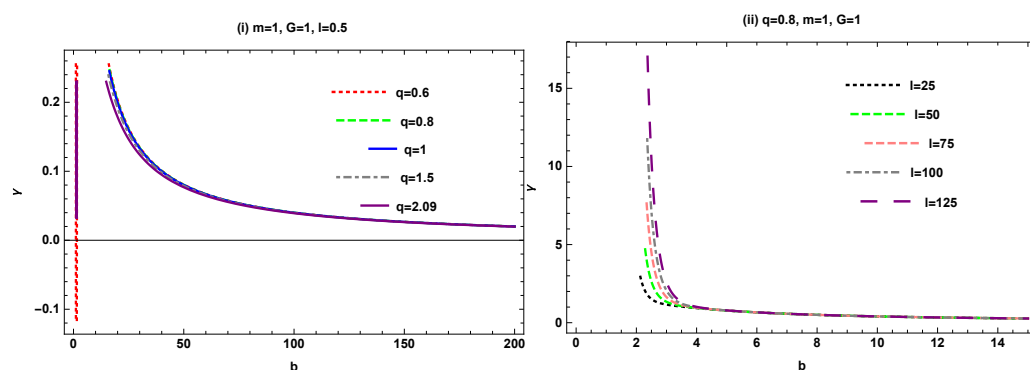


Figure 1. γ in connection with b .

In the first figure, it is observed that deflection angle shows the negative behaviour at $q = 0.6$ and $q = 2.09$ and shows positive behaviour at $0.6 < q < 2.09$ by fixing $G = 1, m = 1$, and $l = 0.5$.

In the second figure, we analysed that the deflection angle gradually decreases and then eventually goes to infinity for large variation of l and fixes $G = 1, m = 1$, and $q = 0.8$, which is the unstable state of magnetized BH. Therefore, we conclude that for small values of l , the MRBH is stable, but as l increases, it shows the unstable behaviour of MRBH. We also observe that at a high value of m , the angle shows the same behaviour.

4.2. Deflection Angle γ versus BH Charge q

Figure 2 shows the behaviour of γ with q by fixing $l = 0.5, G = 1$, and $m = 1$, and varying b . The domain of BH charge is taken to be $0 \leq b \leq 15$.

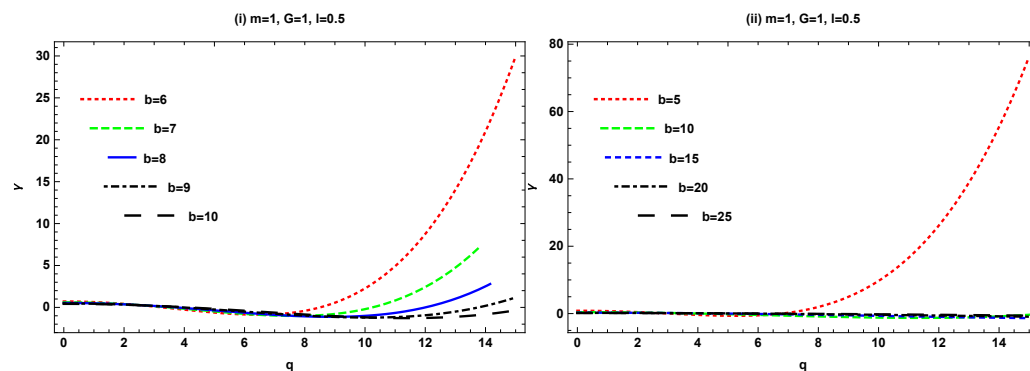


Figure 2. γ in connection with q .

In the left graph, it is observe that deflection angle firstly increase but then for higher values of b the deflection angle is decreased. We also observe that, when we fix greater value of l , the angle shows the same behaviour.

In the right graph, we observed that the deflection angle increases for smaller values of b , but as b increases, the deflection angle become negatively decreased. Furthermore, we observed that the angle shows the same behaviour when we put $m = 150$.

5. Effect of Plasma on Weak Deflection Angle γ for MRBH

In this section, the impact of the angle of deflection by MRBH in plasma medium is examined. We consider the MRBH in plasma, possessing the refractive index [21],

$$n^2(r) = 1 - \frac{\omega_e^2(r)}{\omega_\infty^2(r)} H(r). \tag{20}$$

The corresponding refractive index is expressed as:

$$n(r) = \sqrt{1 - \frac{\omega_e^2}{\omega_\infty^2} H(r)}. \tag{21}$$

Here, ω_e denotes the electron plasma frequency and ω_∞ denotes photon frequency. The corresponding metric function is written as:

$$ds^2 = -H(r)dt^2 + \frac{1}{H(r)}dr^2 + r^2d\Omega_2^2, \tag{22}$$

and

$$H(r) = 1 - \frac{2Gm}{r} + \frac{Gq^2}{r^2} + \frac{4G^2m^2l^2}{r^4} - \frac{4G^2ml^2q^2}{r^5}. \tag{23}$$

In order to study the application of the Gauss–Bonnet theorem to the determination of the bending angle proposed by Gibbons and Werner [18], we considered a two-dimensional Riemannian manifold $(M^{opt}; g_{xy}^{opt})$ with the optical metric $g_{xy}^{opt} = -\frac{n^2}{g_{00}}g_{xy}$. The corresponding optical metric is defined as follows [21]:

$$d\sigma^2 = g_{xy}^{opt} dx^x dx^y = n^2 \left[\frac{dr^2}{H^2(r)} + \frac{r^2 d\theta^2}{H(r)} \right],$$

where $x, y = 1, 2, 3, \dots$

This metric preserves the angle between two curves at a given point and is conformally related to the metric (3), when source and observer are in the tropical region, they possess $\theta = \frac{\pi}{2}$, and we imposed $ds^2 = 0$ in cases of null geodesics.

Gaussian optical curvature \mathcal{K} is examined as:

$$\mathcal{K} = \frac{R_{r\psi r\psi}(g_{xy}^{opt})}{\det(g_{xy}^{opt})}. \tag{24}$$

for simplicity, we let

$$\tilde{\omega} = \frac{\omega_e}{\omega_\infty} \tag{25}$$

By using Equation (24) in the weak field approximation, the Gaussian curvature is expressed as:

$$\begin{aligned}
 \mathcal{K} \approx & \left(-\frac{2}{r^3} - \frac{3\tilde{\omega}^2}{r^3}\right)mG + \left(\frac{3}{r^4} + \frac{5\tilde{\omega}^2}{r^4}\right)q^2G + \frac{100 + 3r^2}{r^6}m^2G^2 \\
 & + \frac{12(15 + r^2)\tilde{\omega}^2}{r^6}m^2G^2 + \left(\frac{-6(25 + r^2)}{r^7} - \frac{(275 + 26r^2)\tilde{\omega}^2}{r^7}\right)mq^2G^2 \\
 & + \left(\frac{2}{r^6} + \frac{(10)\tilde{\omega}^2}{r^6}\right)q^4G^2 - \frac{12(13 + l^2)}{r^7}m^3G^3 + \frac{30(10 + l^2)}{r^8}m^2q^2G^3 \\
 & - \frac{2(362 + 13l^2 + 6r^2)\tilde{\omega}^2}{r^7}m^3G^3 + \frac{2(737 + 34l^2 + 16r^2)\tilde{\omega}^2}{r^8}m^2q^2G^3 \\
 & - \frac{2(47 + 9l^2)}{r^9}mq^4G^3 - \frac{(560 + 42l^2 + 23r^2)\tilde{\omega}^2}{r^9}mq^4G^3 \\
 & + \frac{6(260 - 200l^2 - 6r^2 + 3l^2r^2)}{r^{11}}m^3q^2G^4 - \frac{2(1212)\tilde{\omega}^2}{r^{11}}m^3q^2G^4 \\
 & - \frac{2(1592l^2)\tilde{\omega}^2}{r^{11}}m^3q^2G^4 - \frac{2(941r^2 + 75l^2r^2)\tilde{\omega}^2}{r^{11}}m^3q^2G^4 \\
 & - \frac{2(485 - 360l^2 - 18r^2 + 9l^2r^2)}{r^{12}}m^2q^4G^4 + \frac{4(370)\tilde{\omega}^2}{r^{12}}m^2q^4G^4 \\
 & + \frac{4(480l^2 + 336r^2 + 35l^2r^2)\tilde{\omega}^2}{r^{12}}m^2q^4G^4.
 \end{aligned} \tag{26}$$

By using GBT, the deflection angle was calculated and contrasted to the equation of the angle obtained for non-plasma. Light beams follow a straight line approximation, and we calculated the deflection angle for the plasma.

$$\gamma = - \lim_{R \rightarrow 0} \int_0^\pi \int_{\frac{b}{\sin \psi}}^R \mathcal{K} dS. \tag{27}$$

By using Equation (27), we obtain the angle of the desired BH for the plasma medium, expressed as:

$$\begin{aligned}
 \gamma \approx & \frac{(4Gm)}{b} + \frac{(3G^2m^2\pi)}{4b^2} - \frac{(3Gq^2\pi)}{4b^2} - \frac{(8G^2mq^2)}{3b^3} - \frac{(75G^2m^2\pi)}{8b^4} \\
 & - \frac{(45G^3m^2q^2\pi)}{32b^4} + \frac{(15G^2q^4\pi)}{64b^4} + \frac{(32G^2mq^2)}{b^5} + \frac{(12G^3mq^4)}{5b^5} \\
 & + \frac{(125m^2G^3q^2\pi)}{8b^6} + \frac{(525G^4m^2q^4\pi)}{256b^6} - \frac{(4192G^3mq^4)}{245b^7} \\
 & - \frac{(43155G^4m^2q^4\pi)}{2048b^8} + \frac{(6111G^4m^2q^4\pi)}{256b^{10}} + \frac{(567G^4l^2m^2q^4\pi)}{128b^{10}} \\
 & + \frac{(2Gm)\tilde{\omega}^2}{b} - \frac{(15G^2m^2\pi)\tilde{\omega}^2}{2b^4} - \frac{(G^2m^2\pi)\tilde{\omega}^2}{2b^2} + \frac{(80G^2mq^2)\tilde{\omega}^2}{3b^5} \\
 & + \frac{(2G^2mq^2)\tilde{\omega}^2}{b^3} - \frac{(Gq^2\pi)\tilde{\omega}^2}{2b^2} + \frac{(945G^4l^2m^2q^4\pi)\tilde{\omega}^2}{256b^{10}} \\
 & - \frac{(465G^3m^2q^2\pi)\tilde{\omega}^2}{32b^6} + \frac{(3G^3m^2q^2\pi)\tilde{\omega}^2}{8b^4} + \frac{(4112G^3mq^4)\tilde{\omega}^2}{245b^7} \\
 & - \frac{(2G^3mq^4)\omega^2}{3b^5} - \frac{(3G^2q^4\pi)\tilde{\omega}^2}{16b^4} - \frac{(15435G^4m^2q^4\pi)\tilde{\omega}^2}{256b^{10}} \\
 & + \frac{(14105G^4m^2q^4\pi)\tilde{\omega}^2}{2048b^8} - \frac{(45G^4m^2q^4\pi)\tilde{\omega}^2}{128b^6}.
 \end{aligned} \tag{28}$$

In the case of the plasma medium, the deflection angle γ depends on the m of the BH, q , b , G , and l and on the plasma term. The bending angle obtained in the plasma medium

increases with the parameter $\frac{\omega_e^2}{\omega_\infty^2}$, which shows that lower the photon frequency observe by a static spectator at infinity, greater the deflection angle of it for the fix electron plasma frequency. We also observed that when we take the $q = 0, G = 1,$ and $l = 0,$ the deflection angle obtained in the plasma medium reduces to the deflection angle of the Schwarzschild black hole in the plasma medium. We also investigated that the deflection angle obtained in the plasma medium reduces to the deflection angle that we have obtained in case of non-plasma, when we take $\frac{\omega_e^2}{\omega_\infty^2} = \tilde{\omega} = 0.$

6. Graphical Analysis for Plasma Medium

This section is to study the effect of plasma on deflection angle γ . The physical importance of Figures 3 and 4 are studied. Moreover, we consider $\tilde{\omega} = 10^{-1}$ and give different values to the b and q of the BH, to investigate the behaviour of γ .

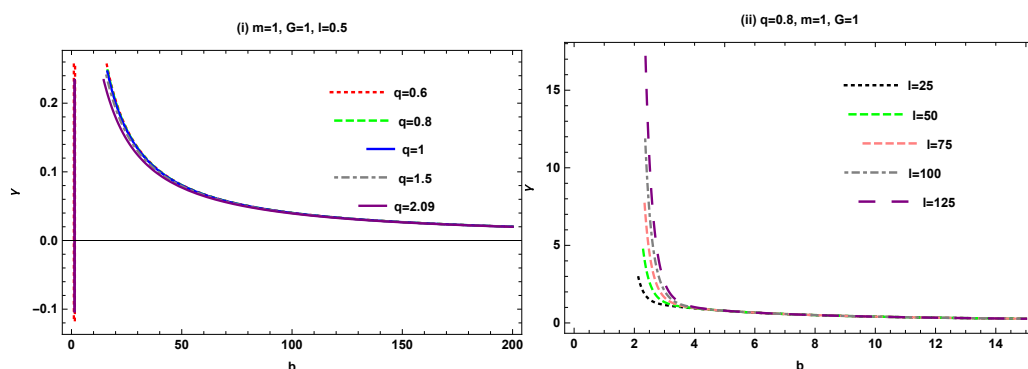


Figure 3. γ in connection with b .

6.1. Deflection Angle γ with Impact Parameter b

In the Figure 3, it is observed that the deflection angle shows negative behaviour at $q = 0.6$ and $q = 2.09$ and shows positive behaviour at $0.6 < q < 2.09$ by fixing $G = 1, m = 1,$ and $l = 0.5.$

In the second figure, we analysed the deflection angle, which gradually decreases and then eventually goes to infinity for large variation of l and fixed $G = 1, m = 1,$ and $q = 0.8,$ which is the unstable state of magnetized BH. Therefore, we conclude that, for small values of $l,$ the MRBH is stable, but as l increases, it shows the unstable behaviour of MRBH. We also observe that, at high value of $m,$ the angle shows the same behaviour.

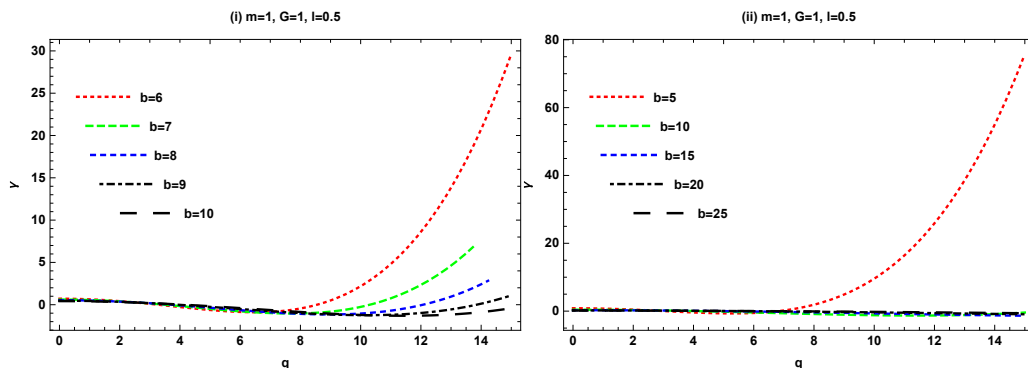


Figure 4. γ in connection with q .

6.2. Deflection Angle γ with BH Charge q

In the left graph of the Figure 4, it is observed that deflection angle firstly increases but then, for higher values of $b,$ the deflection angle decreases. We also observed that, when we fix greater value of $l,$ the angle shows the same behaviour.

In the right graph of the Figure 4, we observed that the deflection angle increases for smaller values of b , but as b increases, the deflection angle become negatively decreased. Furthermore, we found that the angle shows the same behaviour when we put $m = 150$.

7. Derivation of Greybody Factor of MRBH

The MRBH metric in the d -dimension is defined as follows:

$$ds^2 = -H(r)dt^2 + \frac{dr^2}{H(r)} + r^2(d\theta^2 + \sin^2 \theta d\phi^2), \tag{29}$$

where the metric function is defined as:

$$H(r) = 1 - \frac{2Gm}{r} + \frac{Gq^2}{r^2} + \frac{4G^2m^2l^2}{r^4} - \frac{4G^2ml^2q^2}{r^5}. \tag{30}$$

We numerically computed the horizons of the metric $H(r)$ in Figure 5.

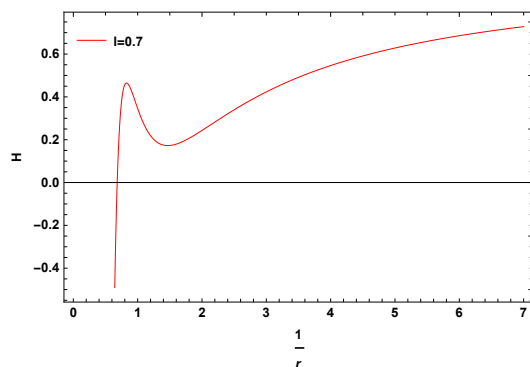


Figure 5. H versus r .

After the computation, the outer horizon of MRBH is $r_+ = 1.6$. The Schrodinger-like equation is defined as follows [35–37]:

$$\left[\frac{d^2}{dr_*^2} + \omega^2 - V(r) \right] \phi = 0, \tag{31}$$

where

$$dr_* = \frac{1}{H(r)} dr, \tag{32}$$

The potential $V(r)$ mentioned in Equation (31) is stated as:

$$V(r) = \frac{(d-2)(d-4)}{4} \frac{H^2(r)}{r^2} + \frac{(d-2)}{2} \frac{H(r)\partial_r H(r)}{r} + l(l+d-3) \frac{H(r)}{r^2}. \tag{33}$$

Greybody factor bound is calculated as using the following Equation [37]:

$$T \geq \text{sech}^2 \left(\frac{l}{2\omega} \int_{r_+}^{\infty} \frac{V(r)}{H(r)} dr_* \right). \tag{34}$$

Then,

$$T \geq \text{sech}^2 \left(\frac{1}{2\omega} \int_{r_+}^{\infty} \left(\frac{(d-2)(d-4)}{4} \frac{H(r)}{r^2} + \frac{(d-2)}{2} \frac{\partial_r H(r)}{r} + \frac{l(l+d-3)}{r^2} \right) dr \right) \tag{35}$$

The Equation (35) is written as when we put $d = 4$,

$$T \geq \text{sech}^2 \left(\frac{1}{2\omega} \int_{r_+}^{\infty} \left(\frac{\partial_r H(r)}{r} + \frac{l(l+1)}{r^2} \right) dr \right) \tag{36}$$

After simplifying the integral, we substituted r_+ ,

$$T \geq \operatorname{sech}\left[\frac{0.625l(l+1) + 0.390625Gm - 0.305176G^2l^2m^2 - 0.16276Gq^2 + 0.198682G^2l^2mq^2}{2\omega}\right]^2. \tag{37}$$

Hence, we obtain the final expression for rigorous bound of the MRBH and observe that it depends on $l, G, q,$ and m and ω .

8. Graphical Study of the Greybody Bound for MRBH

In this section, we analyse the graphical behaviour of greybody bound on MRBH. The physical significance of these plots also shows the effect of parameters on the lower bound by changing the values of the charge of the BH.

Rigorous Bound T_b in Connection with Omega ω

Figure 6 shows the behaviour of T_b with respect to ω when mass $m = 1, l = 0,$ and $G = 1$ are fixed, and gives variation to q . In the left figure, it can be seen that the bound T_b shows constantly increasing behaviour when the domain is taken $0 \leq \omega \leq 1$. In the right figure, it is observed that the obtained bound shows negatively decreasing behaviour when we take the domain $0 \leq \omega \leq 15$.

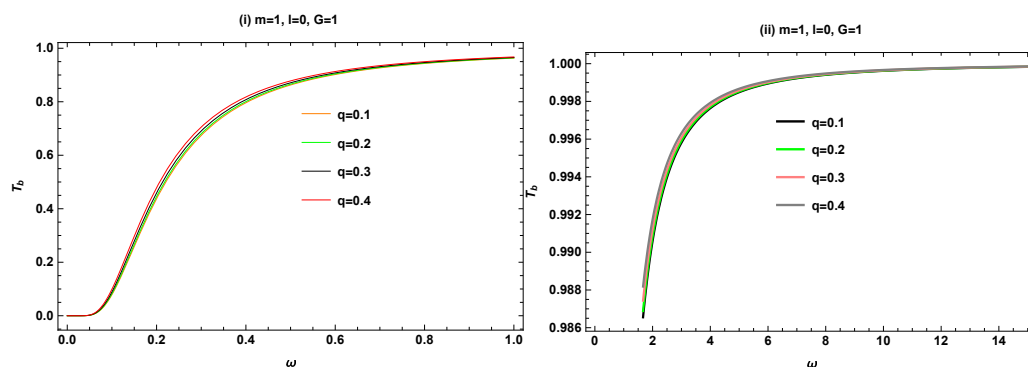


Figure 6. T_b with respect to ω .

9. Conclusions

The current paper explored the deflection angle of MRBH for plasma and non-plasma mediums and greybody bounds. For this purpose, we used GBT and found the deflection angle of the photon.

9.1. Bending Angle γ

(i) Non-plasma Medium:

The deflection angle γ obtained in Equation (19) for non-plasma medium depends on m of the BH, $q, b, G,$ and l . We observe that in the attain deflection angle, the first term is the well-known result for the Schwarzschild black hole, when we put $G = 1, l = 0,$ and $q = 0$.

(ii) Plasma Medium:

In case the of the plasma medium, the deflection angle γ in Equation (28) depends on m of the BH, $q, b, G,$ and l and on the plasma term. The bending angle obtained in the plasma medium increases with the parameter $\frac{\omega_e^2}{\omega_\infty^2}$, which shows that the lower the photon frequency observed by a static spectator at infinity, the greater the deflection angle of it for the fixed electron plasma frequency. We also observe that, when we take the $q = 0, G = 1,$ and $l = 0$, the deflection angle obtained in the plasma medium reduces to the deflection angle of the Schwarzschild BH in plasma medium. We also found that the deflection angle obtained in the plasma medium reduces to the deflection angle that we obtained in case of non-plasma, when we take $\frac{\omega_e^2}{\omega_\infty^2} = 0$.

9.2. Greybody Factor Bounds T

We calculated the rigorous bound T_b in Equation (37) for the greybody factor. We found that the obtained bound of greybody factor depends on the m , G , q , l , and ω .

9.3. Graphical Behaviour

After computing the bending angles, we analysed the graphical behaviour of the bending angles for MRBH in both non-plasma and plasma mediums. We also found that the graphical behaviour exhibits similar results in both non-plasma and plasma mediums. These results are described as follows:

(i) For MRBH:

- **The bending angle γ versus impact parameter b :** The graphical behaviour shows that, when we fix the value of $m = 1$, $l = 0.5$, and $G = 1$, and give variation to q , the deflection angle shows positive behaviour for $0.6 < q < 2.09$ and shows negative behaviour at $q = 0.6$ and $q = 2.09$. Similarly, we observed that the deflection angle is decreasing and eventually goes to infinity for large values of l , and by fixing $m = 1$, $q = 0.8$, and Newton's constant $G = 1$.
- **Bending angle γ versus magnetic charge q :** For the fixed values of $G = 1$, $m = 1$, and $l = 0.5$, the γ angle first increases for small values of b , but for large values of b , the deflection angle decreases.

9.4. Graphical Analysis of Greybody Bound

We investigated the graphical results of the greybody bounds for different values of magnetic charges. We found that the bound constantly increases when ω goes to from zero to one, but the bound shows negative, decreasing behaviour when we chose the maximum value of ω at fixed $G = 1$, $l = 0$, and $m = 1$.

Author Contributions: Conceptualization, W.J. and A.Ö.; methodology, A.Ö.; validation, W.J. and A.Ö.; formal analysis, S.R.; investigation, S.R.; resources, W.J. and A.Ö.; writing—original draft preparation, S.R.; writing—review and editing, W.J. and A.Ö.; visualization, S.R.; supervision, W.J. and A.Ö. All authors have read and agreed to the published version of the manuscript.

Funding: This research received no external funding.

Institutional Review Board Statement: Not applicable.

Informed Consent Statement: Not applicable.

Conflicts of Interest: The authors declare no conflict of interest.

References

1. Einstein, A. Lens-Like Action of a Star by the Deviation of Light in the Gravitational Field. *Science* **1936**, *84*, 506–507. [[CrossRef](#)]
2. Herdeiro, C.A.R.; Lemos, J.P.S. The black hole fifty years after: Genesis of the name. *arXiv* **2018**, arXiv:1811.06587.
3. Ricon, A.; Panotopoulos, G. Quasinormal modes of an improved Schwarzschild black hole. *Phys. Dark Univ.* **2020**, *30*, 100639. [[CrossRef](#)]
4. Abbott, B.P.; Abbott, R.; Abbott, T.D.; Abernathy, M.R.; Acernese, F.; Ackley, K.; Adams, C.; Adams, T.; Addesso, P.; Adhikari, R.X.; et al. GW150914: The Advanced LIGO Detectors in the Era of First Discoveries. *Phys. Rev. Lett.* **2016**, *116*, 131103. [[CrossRef](#)] [[PubMed](#)]
5. Li, S.S.; Mao, S.; Zhao, Y.; Lu, Y. Gravitational lensing of gravitational waves: A statistical perspective. *Mon. Not. Roy. Astron. Soc.* **2018**, *476*, 2220–2229. [[CrossRef](#)]
6. Bartelmann, M.; Schneider, P. Weak gravitational lensing. *Phys. Rep.* **2001**, *340*, 291–472. [[CrossRef](#)]
7. Cunha, P.V.P.; Herdeiro, C.A.R. Shadows and strong gravitational lensing: A brief review. *Gen. Relativ. Gravit.* **2018**, *50*, 42. [[CrossRef](#)]
8. Eiroa, E.F.; Romero, G.E.; Torres, D.F. Reissner-Nordstrom black hole lensing. *Phys. Rev. D* **2002**, *66*, 024010. [[CrossRef](#)]
9. Keeton, C.R.; Kochanek, C.S.; Falco, E.E. The Optical properties of gravitational lens galaxies as a probe of galaxy structure and evolution. *Astrophys. J.* **1998**, *509*, 561–578. [[CrossRef](#)]
10. Sharif, M.; Iftikhar, S. Equatorial gravitational lensing by accelerating and rotating black hole with NUT parameter. *Astrophys. Space Sci.* **2016**, *361*, 36. [[CrossRef](#)]
11. Virbhadra, K.S.; Ellis, G. F. R. Schwarzschild black hole lensing. *Phys. Rev. D* **2000**, *62*, 084003. [[CrossRef](#)]

12. Shaikh, R.; Kocherlakota, P.; Narayan, R.; Joshi, P.S. Shadows of spherically symmetric black holes and naked singularities. *Mon. Not. Roy. Astron. Soc.* **2019**, *482*, 52–64. [[CrossRef](#)]
13. Islam, S.U.; Kumar, R.; Ghosh, S.G. Gravitational lensing by black holes in the 4D Einstein–Gauss–Bonnet gravity. *JCAP* **2020**, *09*, 030. [[CrossRef](#)]
14. Kumar, R.; Ghosh, S.G.; Wang, A. Gravitational deflection of light and shadow cast by rotating Kalb–Ramond black holes. *Phys. Rev. D* **2020**, *101*, 104001. [[CrossRef](#)]
15. Manna, T.; Rahaman, F.; Molla, S.; Bhadra, J.; Shah, H.H. Strong Lensing of a Regular Black Hole with an Electrodynamics Source. *Gen. Relativ. Gravit.* **2018**, *50*, 54. [[CrossRef](#)]
16. Kuhfittig, P.K.F. Gravitational lensing of wormholes in the galactic halo region. *Eur. Phys. J. C* **2014**, *74*, 2818. [[CrossRef](#)]
17. Rahaman, F.; Kalam, M.; Chakraborty, S. Gravitational lensing by stable C-field wormhole. *Chin. J. Phys.* **2007**, *45*, 518.
18. Gibbons, G.W.; Werner, M.C. Applications of the Gauss–Bonnet theorem to gravitational lensing. *Class. Quant. Grav.* **2008**, *25*, 235009. [[CrossRef](#)]
19. Werner, M.C. Gravitational lensing in the Kerr–Randers optical geometry. *Gen. Relativ. Gravit.* **2012**, *44*, 3047–3057. [[CrossRef](#)]
20. Ishihara, A.; Suzuki, Y.; Ono, T.; Kitamura, T.; Asada, H. Gravitational bending angle of light for finite distance and the Gauss–Bonnet theorem. *Phys. Rev. D* **2016**, *94*, 084015. [[CrossRef](#)]
21. Crisnejo, G.; Gallo, E. Weak lensing in a plasma medium and gravitational deflection of massive particles using the Gauss–Bonnet theorem. A unified treatment. *Phys. Rev. D* **2018**, *97*, 124016. [[CrossRef](#)]
22. Ishihara, A.; Suzuki, Y.; Ono, T.; Asada, H. Finite-distance corrections to the gravitational bending angle of light in the strong deflection limit. *Phys. Rev. D* **2017**, *95*, 044017. [[CrossRef](#)]
23. Övgün, A. Weak field deflection angle by regular black holes with cosmic strings using the Gauss–Bonnet theorem. *Phys. Rev. D* **2019**, *99*, 104075. [[CrossRef](#)]
24. Jusufi, K.; Övgün, A. Gravitational Lensing by Rotating Wormholes. *Phys. Rev. D* **2018**, *97*, 024042. [[CrossRef](#)]
25. Jafarzade, K.; Zangeneh, M.K.; Lobo, F.S.N. Shadow, deflection angle and quasinormal modes of Born–Infeld charged black holes. *JCAP* **2021**, *04*, 008. [[CrossRef](#)]
26. Kumaran, Y.; Övgün, A. Deriving weak deflection angle by black holes or wormholes using Gauss–Bonnet theorem. *Turk. J. Phys.* **2021**, *45*, 247–267.
27. Okyay, M.; Övgün, A. Nonlinear electrodynamics effects on the black hole shadow, deflection angle, quasinormal modes and greybody factors. *JCAP* **2022**, *01*, 009. [[CrossRef](#)]
28. Fu, Q.M.; Zhao, L.; Liu, Y.X. Weak deflection angle by electrically and magnetically charged black holes from nonlinear electrodynamics. *Phys. Rev. D* **2021**, *104*, 024033. [[CrossRef](#)]
29. Javed, W.; Hamza, A.; Övgün, A. Effect of nonlinear electrodynamics on the weak field deflection angle by a black hole. *Phys. Rev. D* **2020**, *101*, 103521. [[CrossRef](#)]
30. Hensh, S.; Abdujabbarov, A.; Schee, J.; Stuchlík, Z. Gravitational lensing around Kehagias–Sfetsos compact objects surrounded by plasma. *Eur. Phys. J. C* **2019**, *79*, 533. [[CrossRef](#)]
31. Hawking, S.W. Particle Creation by Black Holes. *Commun. Math. Phys.* **1975**, *43*, 199–220; Erratum in *Commun. Math. Phys.* **1976**, *46*, 206. [[CrossRef](#)]
32. Fernando, S. Greybody factors of charged dilaton black holes in 2 + 1 dimensions. *Gen. Relativ. Gravit.* **2005**, *37*, 461–481. [[CrossRef](#)]
33. Panotopoulos, G.; Rincón, A. Greybody factors for a minimally coupled scalar field in three-dimensional Einstein–power–Maxwell black hole background. *Phys. Rev. D* **2018**, *97*, 085014. [[CrossRef](#)]
34. Konoplya, R.A.; Zinhailo, A.F. Grey-body factors and Hawking radiation of black holes in 4D Einstein–Gauss–Bonnet gravity. *Phys. Lett. B* **2020**, *810*, 135793. [[CrossRef](#)]
35. Boonserm, P.; Visser, M. Bounding the Bogoliubov coefficients. *Ann. Phys.* **2008**, *323*, 2779–2798. [[CrossRef](#)]
36. Boonserm, P. Rigorous bounds on Transmission, Reflection, and Bogoliubov coefficients. *arXiv* **2009**, arXiv:0907.0045.
37. Boonserm, P.; Visser, M. Bounding the greybody factors for Schwarzschild black holes. *Phys. Rev. D* **2008**, *78*, 101502. [[CrossRef](#)]
38. Boonserm, P.; Chatrabhuti, A.; Ngampitipan, T.; Visser, M. Greybody factors for Myers–Perry black holes. *J. Math. Phys.* **2014**, *55*, 112502. [[CrossRef](#)]
39. Otorola, G.; Övgün, A.; Saavedra, J.; Videla, N. Inflation from a nonlinear magnetic monopole field nonminimally coupled to curvature. *JCAP* **2018**, *06*, 003. [[CrossRef](#)]
40. Born, M.; Infeld, L. Foundations of the new field theory. *Proc. Roy. Soc. Lond. A* **1934**, *144*, 425–451. [[CrossRef](#)]
41. Frolov, V. Weakly magnetized black holes as particle accelerators. *Phys. Rev. D* **2012**, *85*, 024020. [[CrossRef](#)]
42. Kruglov, S.I. Regular model of magnetized black hole with rational nonlinear electrodynamics. *Int. J. Mod. Phys. A* **2021**, *36*, 2150158. [[CrossRef](#)]